Nano Energy 26 (2016) 360–370

Contents lists available at ScienceDirect

Nano Energy

journal homepage: www.elsevier.com/locate/nanoen

Surface dipole enhanced instantaneous charge pair generation in triboelectric nanogenerator

Kyeong Nam Kim [a], Yun Kyung Jung [b], Jinsung Chun [a], Byeong Uk Ye [a], Minsu Gu [b], Eunyong Seo [b], Seongsu Kim [d], Sang-Woo Kim [d,e], Byeong-Su Kim [b,c,*], Jeong Min Baik [a,*]

[a] School of Materials Science and Engineering, KIST-UNIST-Ulsan Center for Convergent Materials, Ulsan National Institute of Science and Technology (UNIST), Ulsan 689-798, Republic of Korea
[b] Department of Energy Engineering, Ulsan National Institute of Science and Technology (UNIST), Ulsan 689-798, Republic of Korea
[c] Department of Chemistry, Ulsan National Institute of Science and Technology (UNIST), Ulsan 689-798, Republic of Korea
[d] School of Advanced Materials Science and Engineering, Sungkyunkwan University (SKKU), Suwon 440-746, Republic of Korea
[e] SKKU Advanced Institute of Nanotechnology (SAINT), Sungkyunkwan University (SKKU), Suwon 440-746, Republic of Korea

ARTICLE INFO

Article history:
Received 21 April 2016
Received in revised form
23 May 2016
Accepted 27 May 2016
Available online 30 May 2016

Keywords:
Dmap-Au
Charge transfer
Stretchable
Triboelectric
Nanogenerator

ABSTRACT

Developing a successful strategy to maximize the surface charge density is crucial to speed-up the commercialization success of triboelectric nanogenerator. Here, for the first time, the fabrication of positive triboelectric material to donate electrons efficiently to dielectrics is reported, by increasing the stretchability for the uniform contact and by introducing a functional group for the surface potential control. A highly stretchable and conductive film with Ag nanowires and PDMS was fabricated as a base material, in which the portion of nanowires exposed above the embedding surface should be accurately controlled. In specific, positively charged 4-(dimethylamino)pyridine (DMAP) coated Au nanoparticles, prepared by phase transfer method, are coated. The DMAP lowers the effective work function of the nanoparticles by a permanent dipole induced at the DMAP-Au interface and enhances the electron transfer to the dielectrics, confirmed by the Kelvin probe force microscope measurement. The designed nanogenerator gives an output performance up to 80 V and 86 μA, and 2.5 mW in output power, 2.5 times enhancement compared with the conventional TENG. With the integration with AC to DC converting circuit and buck-boost circuit, the nanogenerator produces a constant voltage of 2.6 V. The wireless sensing system, which operates the remote controller, were also demonstrated, turning on a siren.

1. Introduction

Contact electrification is a phenomenon in which electrical charge (generally considered as electron) is transferred between the two materials when they are brought into contact. The contact electrification has been successfully applied in several useful technologies, such as photocopying [1], laser printing [2], and electrostatic separation [3]. Very recently, a new type of power generating device, termed as the triboelectric nanogenerator (TENG) [4–7], based on triboelectric effects coupled with electrostatic effects, has been demonstrated. So far, TENGs have been successfully proven as a cost-effective, simple, and robust technique in realizing many self-powered applications.

Despite the successful development and demonstration of the TENGs, the output power may be still low and requires further enhancement to speed up the commercialization for certain applications. To date, most of the reports have focused on the surface patterning and device structure to enhance the output power [8–11]. Very few reports have been brought to the negative triboelectric materials (i.e. dielectrics) such as the increase of the compressibility [12] and surface potential control [13,14], to enhance the capability of gaining electrons and sustaining them on the surface. However, there was few report on the functional modification of positive triboelectric materials [15] despite the importance of electron-donating property on the output performance. As positive triboelectric materials, various metals such as aluminum (Al), copper (Cu), and gold (Au) in rigid thin film form have been mainly used [16–20], however, the charge transfer may not be efficient due to the non-uniform contact surface and the non-uniform potential distribution on the surface occurring because of surface heterogeneity, decreasing the effective density of the charges. Although there have been a few papers on stretchable positive triboelectric materials [21,22], they do not show a facile way to control the surface potential.

* Corresponding authors.
E-mail addresses: bskim19@unist.ac.kr (B.-S. Kim), jbaik@unist.ac.kr (J.M. Baik).

http://dx.doi.org/10.1016/j.nanoen.2016.05.048
2211-2855/

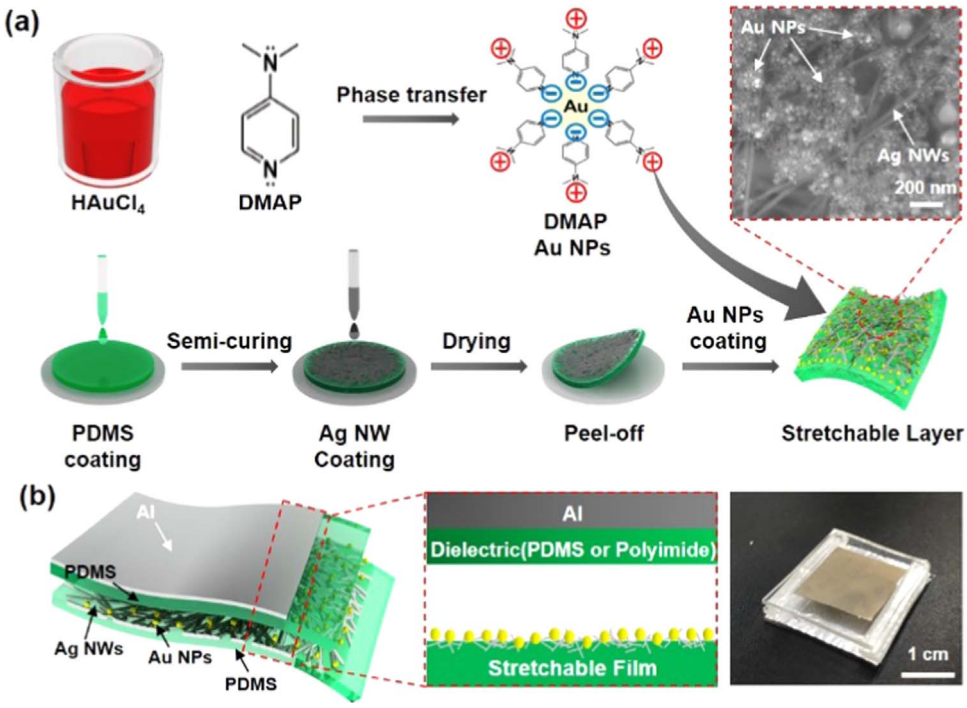

Fig. 1. (a) Schematic illustration (top side) and SEM image (right side) of the Au NPs capped with DMAP from phase transfer method. The fabrication method of DMAP-Au NPs-supported stretchable film which is a PDMS film embedded with Ag NWs (bottom side). (b) Schematic and photographic images of the stretchable TENG.

The functional groups on the surface of metals (in nanoparticle form) such as Au have been considered to effectively change the surface potential by the conjugation with ionic ligands [23–25]. With the molecule bound to the nanoparticles (NPs), negative or positive charges reside on the outside of the particle making highly charged surface, thereby, changing the surface potential. Based on this strategy, here, we develop a positive triboelectric material to donate electrons efficiently to the dielectrics, such as polydimethylsiloxane (PDMS) and polyimide. The positive triboelectric material composed of mainly 4-(dimethylamino)pyridine (DMAP)-capped Au NPs, Ag nanowires (NWs), and PDMS. The Ag NWs are partially embedded in the PDMS and the portion of exposed was precisely controlled to improve the stability of the material during the physical contact as well as enhance the charge transfer. In specific, the DMAP ligand of Au NPs are decorated on the Ag NWs-PDMS film. The DMAP was found to lower the effective work function of the Au NPs because of an interfacial dipole within a few nanometers, induced from partial protonation of the exocyclic nitrogen atom that extends away from the surface of the Au NPs. This increases the work function difference with the dielectrics, thereby, increasing the charge density on both surfaces. To support the results, OH- and citrate-modified Au NPs were also prepared. We confirmed it by measuring and comparing the surface potentials of the dielectrics before and after friction by the Kelvin probe force microscope (KPFM).

The designed TENG gave an output performance up to 80 V and 86 μA, and 2.5 mW in output power, 2.5 times enhancement compared with the conventional TENG. With the integration with AC to DC converting circuit and buck-boost circuit, the TENG is demonstrated to produce a constant voltage of 2.6 V. The wireless sensing system was also demonstrated by the output voltage from the TENG, which operates the remote controller, resulted in turning on a siren of the system.

2. Experimental

2.1. Fabrication of Ag NWs-embedded within PDMS film

Ag NWs (Blue Nano, Inc.) and PDMS (Sylgard 184, Dow Corning) were used for the fabrication of stretchable film. The base monomer (Sylgard 184A) and curing agent (Sylgard 184B) were mixed with a weight ratio of 10: 1, placed into the vacuum desiccator to degas the PDMS mixture. After 30 min, 1 mL of mixture was poured onto the SiO_2/Si substrate, and allowed to solidify into an amorphous free-standing film by heating on an oven at 90 °C for 5 min. Ag NWs was subsequently coated on the PDMS, anchoring the NWs within the PDMS matrix before the film is fully solidified.

2.2. Fabrication process of Au NPs capped with DMAP, OH, and citrate

The DMAP-Au NPs were described previously [26]. Briefly, $HAuCl_4 \cdot 3H_2O$ (30 mL, 30 mM) was added to a 25 mM solution of tetraoctylammonium bromide (TOAB) in toluene (80 mL). A 0.40 M solution of freshly prepared $NaBH_4$ (25 mL) was added to the mixture, causing an immediate reduction. After 30 min, the two phases were separated and the toluene phase was subsequently washed each three times with 0.10 M H_2SO_4, 0.10 M NaOH, and H_2O, and then dried over anhydrous Na_2SO_4. An aqueous DMAP solution (0.10 M, 50 mL) was added to aliquots (50 mL) of the as-prepared NPs mixtures. Direct phase transfer across the organic/aqueous boundary was completed within 1 h without additional stirring and the DMAP-Au NPs in aqueous phase were obtained.

OH-modified Au NPs were prepared by the modified method [27–29]. An aqueous solution of $HAuCl_4 \cdot 3H_2O$ (30 mL, 30 mM) was mixed with a solution of TOAB in toluene (35 mL, 25 mM). The two-phase mixture was vigorously stirred until all the tetrachloroaurate was transferred into the organic layer. Dodecanethiol (DDT, $CH_3(CH_2)_{11}SH$, 4.2 mmol) was then added to the organic

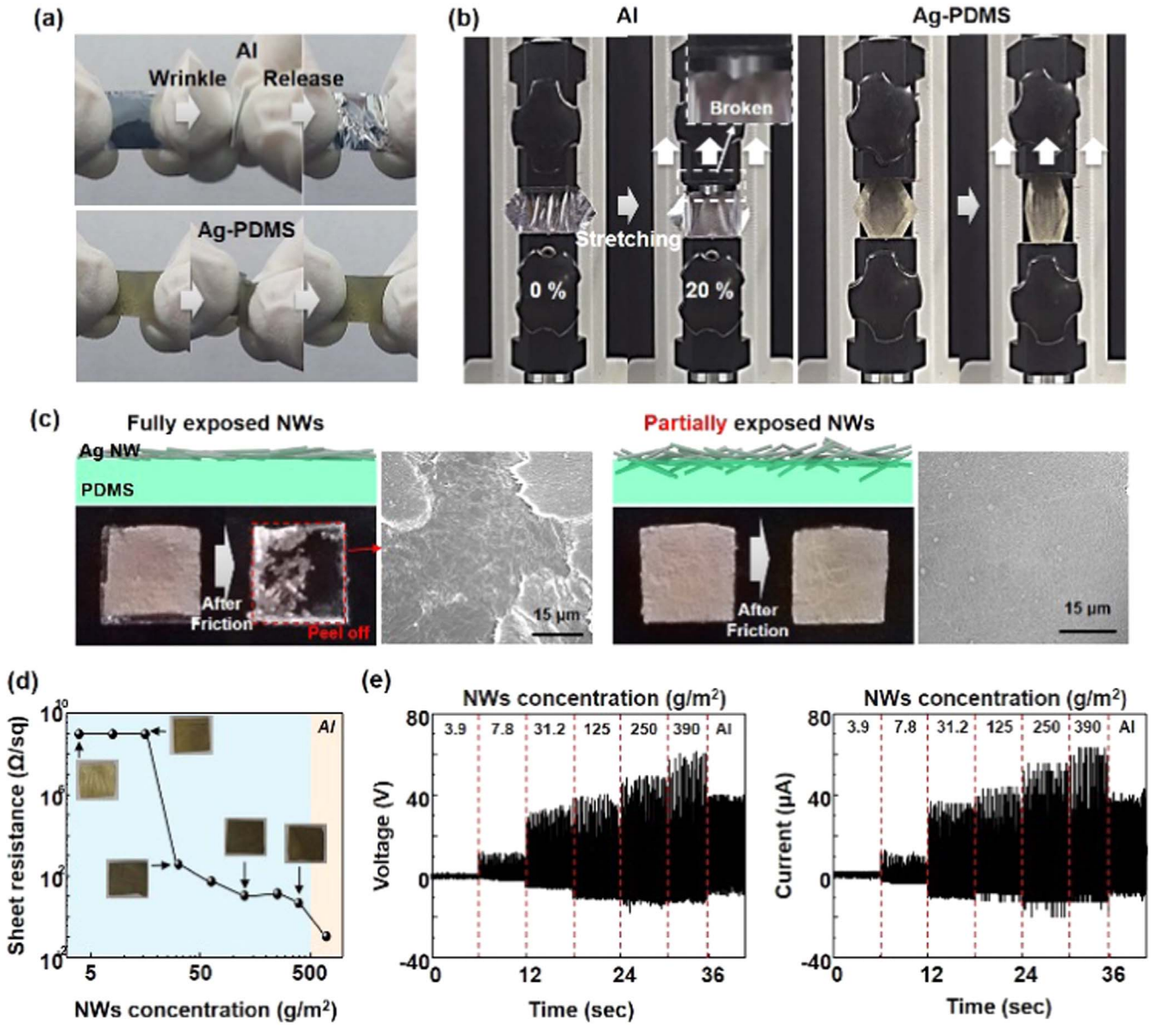

Fig. 2. (a) The photographs of wrinkle test of Al film (top side) and Ag-PDMS stretchable film (bottom side), (b) the snapshot of stretchable test of Al film (left side) and Ag-PDMS stretchable film (right side). (c) The schematic images of fully- and partially-exposed Ag NWs on PDMS. The photographs and SEM images show the stability of the two films. Fully-exposed film was peeled off after friction several times. (d) Sheet resistance of Ag NWs-PDMS as a function of Ag NW concentration. The photographs of the films are also shown in the inset. (e) The output voltage and current of the TENG fabricated with the stretchable film as a function of the concentrations of Ag NWs.

phase. A freshly prepared aqueous solution of $NaBH_4$ (25 mL, 0.4 M) was slowly added with vigorous stirring. After further stirring for 3 h, the organic phase was separated. The solution was extracted with 0.1 M H_2SO_4, 0.1 M NaOH, and H_2O three times and the water was completely removed by Na_2SO_4. After filtering the toluene solution with paper, excess DDT was removed by dilution of DDT-coated Au NPs (8 mL) with an excess of methanol (40 mL, 5 times). And, the solution spun down and resuspended in 2 mL toluene by brief sonication. DDT-Au NPs in toluene (2 mL) was added to thiol-PEG-hydroxyl (PEG 1 K, 10 mg) in 0.5 mL toluene at 70 °C and stirring continued until visible aggregation was observed (within 15 min). Solution was allowed to settle and cooled to RT. The aggregates were washed with toluene twice via decantation and the remaining toluene was removed by drying in vacuum oven. The product was resolved with distilled water.

Au NPs by citrate were synthesized by a modified process [30]. The Au NPs with 5 nm of size were synthesized as a seed. A 20 mL aqueous solution containing $HAuCl_4$ (0.25 mM) and citrate (0.25 mM) was prepared. After the addition of ice-cold, freshly prepared $NaBH_4$ (0.60 mL, 0.10 M), the solution turned pink indicating the formation of spherical Au NPs.

2.3. Fabrication of triboelectric nanogenerator

An 0.40 mL of a 60 mg/L Au NPs dispersion in DI with various surface potentials were casted into a film shape in a blocking layer on sliver NWs based stretchable metal (2 cm × 2 cm) on 24 h at RT. To fabricate the Au NPs decorated stretchable triboelectric nanogenerator, the Al top electrode was attached on PDMS substrate and 100 μm-thick pure PDMS or polyimide film was produced on the Al electrode attached by the double sided polyimide tape. And then, the Au NPs decorated stretchable film was attached on the PDMS substrate.

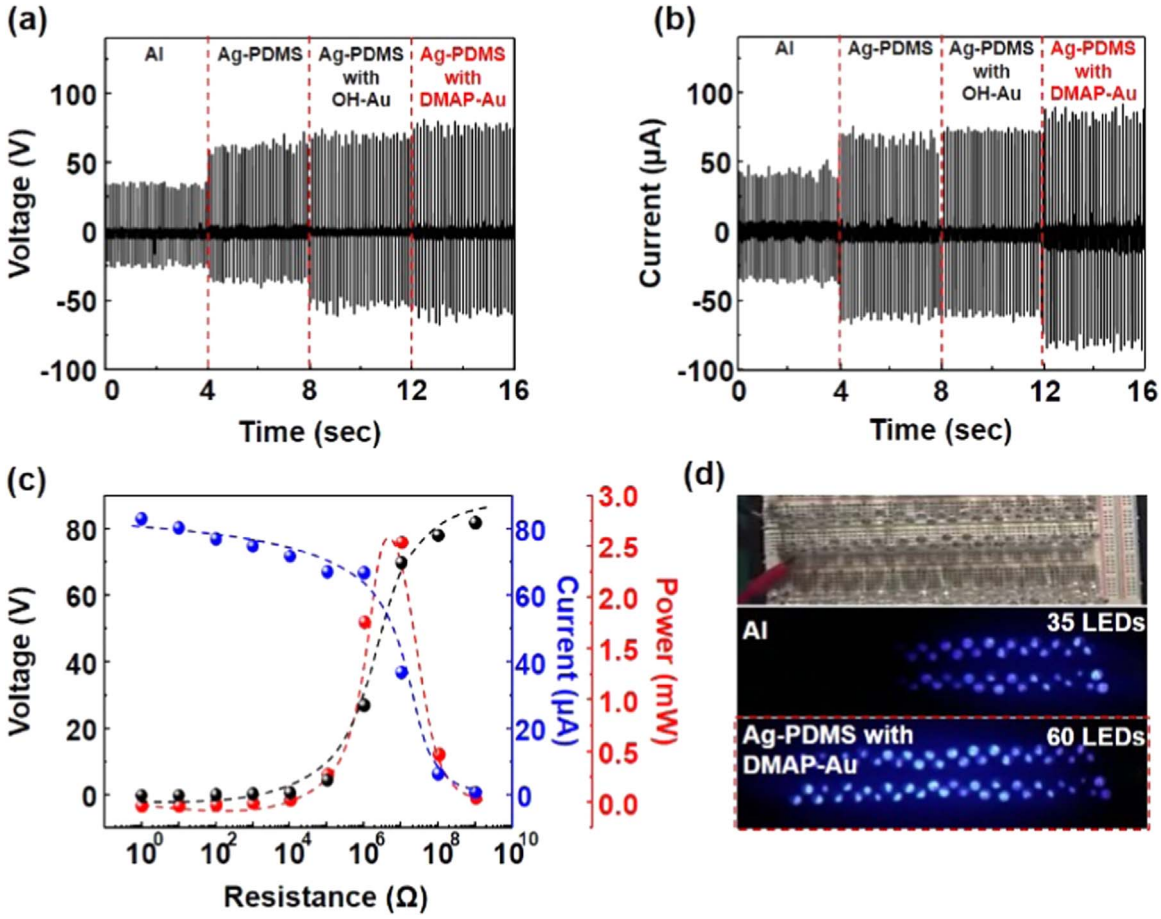

Fig. 3. (a) The output voltages and (b) currents of the TENG with Al film, PDMS film with Ag NWs, and OH- and DMAP-Au NPs supported Ag-PDMS film. (c) The output voltage and current, and output power with resistance of external loads from 10 Ω to 1 GΩ. (d) Snapshots of 60 commercial blue LEDs connected in series by the TENG fabricated with Al, and DMAP-Au NPs supported Ag-PDMS film.

2.4. Characterization and measurements

We measured the output voltage and currents of the TENGs under a vertical compressive strain, measured by a Tektronix DPO 3052 Digital Phosphor Oscilloscope and low-noise current pre-amplifier (model no. SR570, Stanford Research Systems, Inc.). A pushing tester (Labworks Inc., model no. ET-126-4) was used to create vertical compressive force in the nanogenerator. The morphologies of the Au NPs decorated Al film were characterized by a Nano 230 field-emission scanning electron microscope (FEI, USA). Ultraviolet photoelectron spectroscopy (UPS) (Thermo Fisher, ESCALAB 250Xi) was performed using the He I photon line of a He discharge lamp under ultra-high vacuum conditions for the measurement of the work function. Kelvin prove force microscope (KPFM) measurements were also performed using Park systems XE-100 with Pt/Cr-coated silicon tips (tip radius: <25 nm, force constant: 3 N m^{-1}, and resonance frequency: 75 kHz). KPFM images (3 μm × 3 μm) were scanned at a scanning speed of 0.5 Hz, and set at a point of 13 nm from a sample in atmospheric pressure at room temperature. The Zeta potential of Au NPs suspensions was measured using a Zeta potential analyzer (Malvern, Zetasizer nano-zs).

3. Results and discussion

The schematic diagram of the fabrication process of Au NPs-decorated stretchable film is shown in Fig. 1 and the detail information described in Section 2. The Au NPs capped with DMAP was prepared by phase transfer method [26] and Au NPs capped with citrate and OH were prepared by modification of previously reported methods [27–30], in stable aqueous solution. The resultant Au NPs have an average diameter of approximately 6 nm with various surface potentials of +35, 0, and −30 mV. Finally, the Au NPs are decorated on the Ag NWs-PDMS film, as shown in SEM image of Fig. 1a. To fabricate the nanogenerator, the stretchable layer was anchored on the spacer with the top electrode facing up. The spacer was made of insulating polymer, keeping the film at a distance of 1 mm away from the PDMS layer underneath, as shown in Fig. 1b. As a reference, the Al layer without the Au NPs was also prepared.

Fig. 2a and b shows the durability test of the stretchable film, compared with the Al foil typically used as a positive triboelectric material. As expected, the Al is irreversibly deformed by wrinkling on both sides of the Al foil. The stretchable film is reversible to the extreme deformation, as shown in Fig. 2a. Fig. 2b shows the photographs of stretching test with a length increase of over 20%. It is clearly seen that the stretchable film can almost perfectly recover its original shape after release of the tensile force, while the Al foil is broken, unable to withstand the tensile force. This will cause the non-uniform contact, thereby, non-uniform charges will be generated. With these durability tests, in TENG, a periodic external force is applied to the electrode for the energy harvesting, which requires the stability of the film during the physical contact for a long time. As seen clearly, the Ag NWs are partially embedded within the PDMS, leaving the rest of the NWs exposed. The accurate control of the rest is found to be critical to improve the stability of the TENG. Actually, when the exposed NWs are too

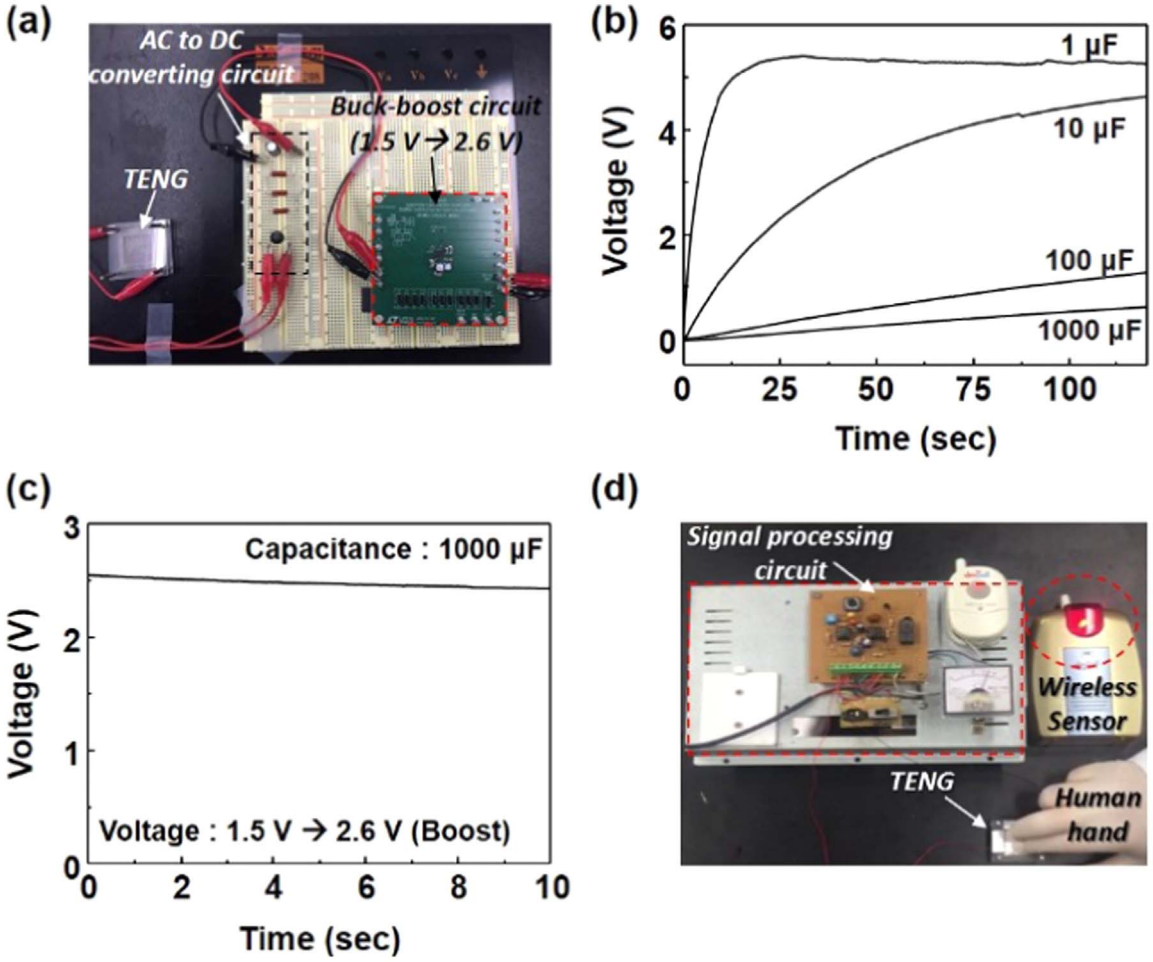

Fig. 4. (a) The photograph of charging system integrated the TENG with buck-boost circuit and AC to DC signal converting circuit. (b) The measured voltage of a commercial capacitor (1, 10, 100, 1000 μF) charged with AC to DC signal converting circuit, (c) The boosted voltage using buck-boost circuit obtained by using 1000 μF. (d) The photograph of wireless sensing system by integrating the TENG with a signal-processing circuit.

long, i.e. if the NWs are coated on the surface of the PDMS, the film is found to peel-off after several pushing-release cycles. However, our film showed very stable performance over 1 day at large pushing force of 90 N, as shown in the Fig. 2c.

As the concentration of Ag NWs increases, the sheet resistance decreases up to ~10 Ω/sq, as shown in Fig. 2d. Although it is still larger than that (~0.1 Ω/sq) of Al film, it is quite conductive, comparable to those reported previously [31–33]. We measured the output voltage and current of the TENG fabricated with the stretchable films as a function of the concentration of the NWs under a compressive force of 50 N and a frequency of 10 Hz, as shown in Fig. 2e. As a negative triboelectric material, PDMS was used. Open-circuit voltage (V_{oc}) and short-circuit current (I_{sc}) were measured to characterize the TENGs' electric performance. The size of the active area is approximately 1.5 cm × 1.5 cm. Compared with that (~0.045 mA) of the TENG fabricated by the Al film, the smaller output currents were measured at lower concentration than 7.8 g/m^2. However, as the concentration of Ag NWs increases, the output current significantly increases up to 0.065 mA. This observation clearly indicates that the electrical signal is originated from the charge transfer between Ag and PDMS. The significant increase of the output current may also be ascribed to the increase of the contact area between the Ag NWs and PDMS film. Also, when the Ag NWs are fully embedded inside PDMS, the output current was very low because of no exposure of Ag NWs on the surface of PDMS film as shown in Fig. S1.

As OH-modified Au NPs were decorated on the Ag-PDMS film and the TENG was fabricated. However, there is no significant enhancement in the output voltage and current although the V_{oc} increased by 10%, as shown in Fig. 3a and b. However, when the Au NPs were capped with DMAP, it was clearly seen that the output current was enhanced to 0.082 mA and 80 V in the I_{sc} and V_{oc}, respectively. To investigate the output power of the TENG, resistors were used as external loads from 10 Ω to 1 GΩ, the instantaneous power of the external resistance for TENG reaches a peak value of 2.6 mW at a resistance of 10 MΩ, as shown in Fig. 3c. By using the TENG, 60 blue LEDs can be lit up during the pushing force in the TENG, compared with that (35 LEDs) by the TENG with Al film (Fig. 3d). The long-term stability of the TENG was also evaluated by using a pushing tester for 24 h. The consistent output current of the TENG were maintained, as shown in Fig. S2.

To show the practical application, we evaluated the charging characteristic of the TENG, which was integrated with AC to DC converting circuit and buck-boost circuit, as shown in Fig. 4a. The converting circuit consists of one rectifier, three low capacitors (3 × 0.001 μF) and one capacitor (1, 10, 100, 1000 μF) to convert AC to DC output signal. When the vertical compressive force of 50 N under frequency of 10 Hz was applied, the capacitors were found to be charged, as shown in Fig. 4b. The measured voltage of the capacitor is also boosted up a constant voltage of 2.6 V using buck-boost circuit, as shown in Fig. 4c. Additionally, an integrated wireless sensing system was developed by integrating the TENG with a signal-processing circuit, as shown in Fig. S3. The wireless

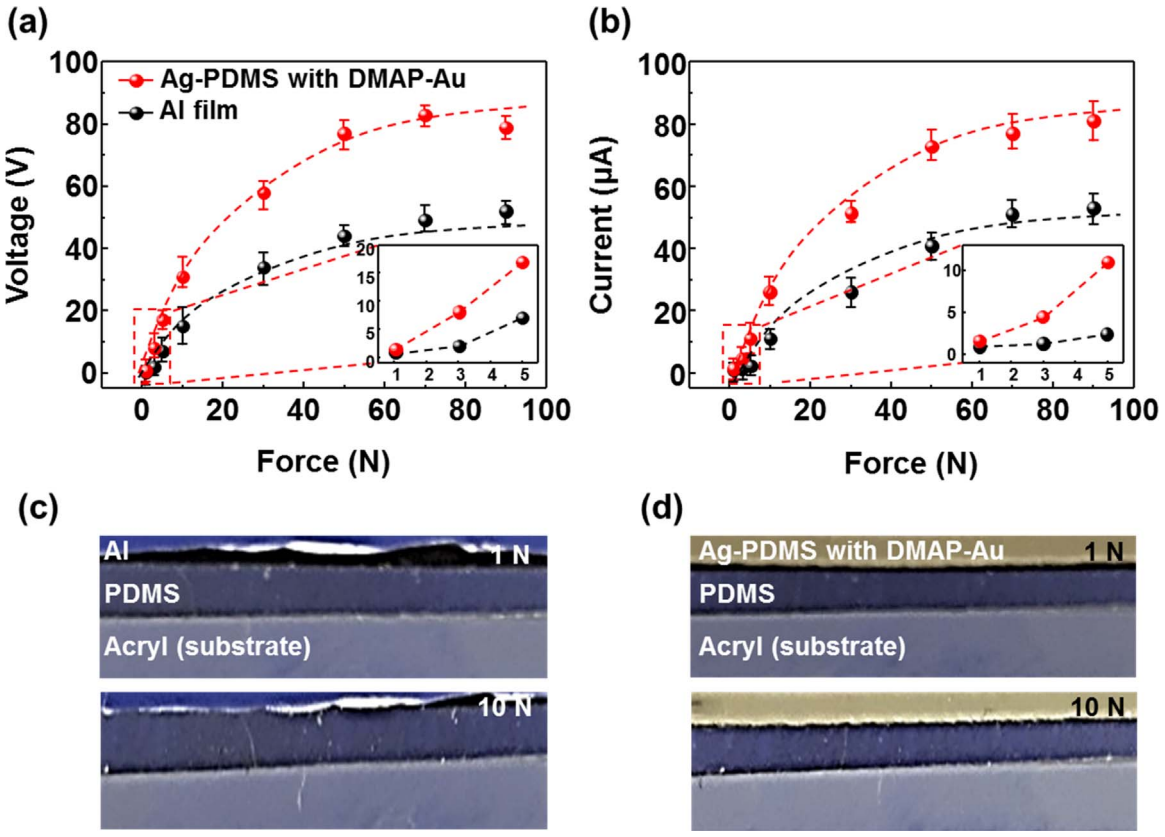

Fig. 5. The output voltages (a) and currents (b) of the TENGs with Al film, Ag-PDMS film coated by DMAP-Au NPs as a function of compressive force. The photographs of contact surface between PDMS and (c) Al, and (d) Ag-PDMS film.

sensing system can be operated by the output voltage from the Au NPs-decorated TENG to trigger an IC timer (NE 555) that controls a wireless transmitter for remotely switching a siren between a emergency and a normal state. When a human hand contacted the TENG, the generated output voltage operates the remote controller, resulted in turning on a siren with flashing light of sensor, as shown in Fig. 4d (also see the movie of Fig. S4).

Supplementary material related to this article can be found online at doi:10.1016/j.nanoen.2016.05.048.

The enhancement in output power of the TENG with the stretchable film coated by DMAP-Au NPs can be explained by the improvement of the contact uniformity and the change of the surface potential. We systematically measured the output performance of the TENG with the stretchable film as a function of external force from 1 N to 90 N, compared with that with Al foil, plotted in Fig. 5a and b. For the TENG with the stretchable film, as the force increases, the output voltage and current increase to 80 V and 0.082 mA, respectively, enhanced by approximately 60% compared with that with Al foil. Here, it is noteworthy that under lower force than 10 N, the output performance steeply increases with the force in the TENG fabricated with the stretchable film, while that with Al foil does not. This indicates that the enhancement is much larger at low forces in the TENG with the stretchable film. Actually, in Figs. 5c and d, the Al foil shows non-uniform contact with PDMS even at a force of 10 N, while the Ag-PDMS film shows quite uniform contact irrespective of the applied force. The non-uniform contact makes the non-uniform charging, decreasing the output power.

Compared with the OH-coated Au NPs, the outer surface of Au NPs carrying a nucleophile such as DMAP has a positive charge and excess electron is transferred to the interior of the NPs, becoming negative. This will induce a permanent dipole at the DMAP–Au interface, pointed away from the surface of Au NPs. The dipole introduces a dipole-induced potential step at the interface when the Au NPs contact with the PDMS, up-shifting the vacuum level in DMAP-coated Au NPs. The change in the work function, $\Delta\Phi_S$, is generally related to the dipole through the Helmholtz equation [34];

$$\Delta\Phi_S = 4\pi \frac{NP_0 \cos\theta}{A\varepsilon \bullet \varepsilon_0}$$

where P_0 is the dipole moment of the free molecular in vacuum state, N/A is the number of dipoles/molecules per surface area, $\varepsilon = (P_0/P)$ is the effective dielectric constant of a molecular monolayer and ε_0 is the permittivity in vacuum. θ is the tilted angle of interfacial dipoles/molecule relative to the surface plane. Thus, the potential step will decrease the effective metal work function in DMAP-coated Au NPs.

Au NPs with different zeta potentials by capping the DMAP, OH, and citrate were prepared and the resultant DMAP-, OH-, and citrate-coated Au NPs were measured to have a surface potential of +35 mV, 0 mV, and −30 mV, respectively, as shown in Fig. 6a. Ultraviolet photoelectron spectroscopy (UPS) measurements were performed to measure the change of the work function respect to the capping agents (Fig. 6b). The work function (Φ_S) can be determined from the secondary electron threshold energy as $\Phi_S = h\nu - (E_{cutoff} - E_F)$. E_{cutoff} is extracted using a linear extrapolation of the high-binding-energy cutoff region of the UPS spectra. The onset of secondary electron peak shifted toward higher binding energy by 0.10 eV as the DMAP ligand was used, compared with the OH-coated Au NPs. As the sodium citrate was capped, it shifted toward lower binding energy by 0.15 eV. Based on these results, it is clearly seen that the smallest work function of approximately 4.43 eV was measured in DMAP-coated Au NPs (Fig. 6c). Fig. 6d shows the energy band diagram at the interface when the Au NPs contact with the PDMS. The permanent dipole of citrate-modified

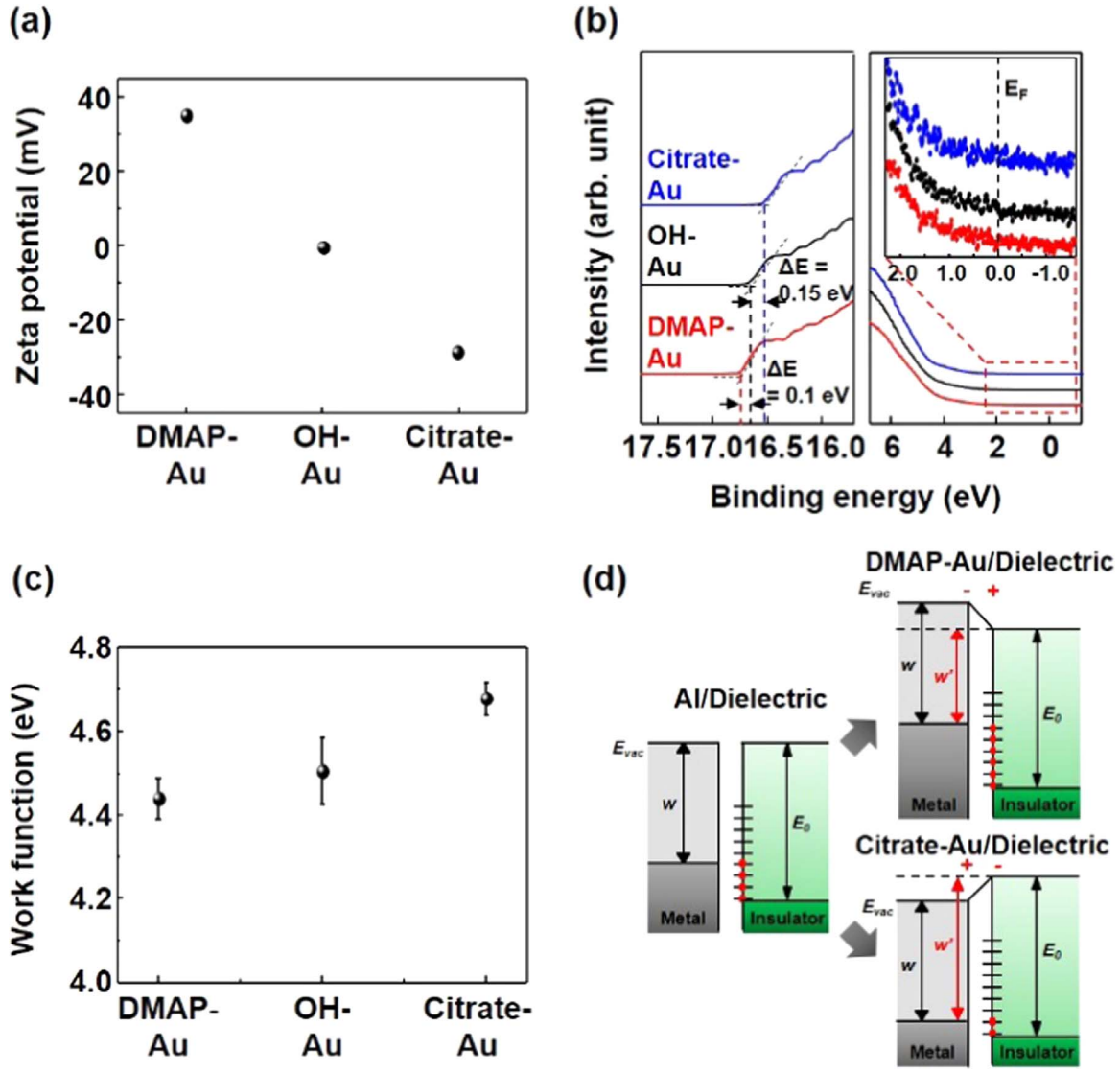

Fig. 6. (a) The Zeta potential of DMAP-, OH-, Citrate-Au NPs. (b) UPS spectra and (c) the change of work function of DMAP-, OH- and Citrate-Au NPs. (d) Energy band diagrams at the Au/PDMS interface during the contact.

Au NPs, in which the dipole are oriented toward the Au NPs, down-shifts the vacuum level, increasing the effective metal work function, whereas the outer surface of DMAP-Au NPs has positive charges, which decreases the effective metal work function. This will account for the increased potential difference with the Fermi level of the PDMS (Fig. 6d).

Finally, the Au NPs with the various capping agents are decorated on the Al films and TENGs are fabricated, the electrical output voltages and currents were measured, plotted in Fig. 7a and b. Compared with the TENG with Al film, the TENG with a citrate as a capping agent showed larger enhancement in the power generation, which is due to the increase in the effective contact area by the Au NPs coating. As the Au NPs were capped with DMAP, it is obvious that the output voltage and current density significantly increase and reach a record value of 63 V and 0.068 mA, respectively. For the transferred charge density, as expected, TENG with Au NPs capped with the DMAP showed the largest value, reaching up to 19 $\mu C/m^2$ under the same mechanical force, as shown in Fig. 7c.

On the basis of the above results, the enhancement in the electrical output performance of Au NPs-decorated TENG can be understood by the increase in the transferred charge density on the surface of the Au NPs and the PDMS, as shown in the COMSOL simulations in Fig. 7d. When the Au NPs-decorated TENG is fully released, if we assume the electric potential (U_{bottom}) of the surfaces of bottom PDMS layer to be zero, the electric potential of the surfaces of top PDMS layer (U_{top}) can be expressed by $U_{top} = \sigma d_{gap}/\varepsilon_0$, where σ is the triboelectric charge density, ε_0 is the vacuum permittivity of free space (8.854×10^{-12} F/m), and the gap distance (d_{gap}) of the TENG can be calculated as $d_{gap} = 0.3$ mm. Thus, the calculated surface charge density (σ) on the surfaces of top PDMS layer can be obtained by $\sigma_{DMAP} = \varepsilon_0 V/d_{gap} = 22.14\ \mu C/m^2$, in which V is the output voltage (150 V) of TENG with Au NPs capped with the DMAP. The maximum surface charge density (σ'_{max}) accumulated on the top electrode can be expressed as below [35].

$$\sigma'_{max} = \frac{\sigma d_{gap} \varepsilon_{PDMS} \varepsilon_{Au}}{d_{PDMS} \varepsilon_{Au} + d_{gap} \varepsilon_{Au} \varepsilon_{PDMS} + d_{Au} \varepsilon_{PDMS}}$$

where ε_{PDMS} and ε_{Au} are the relative permittivity of PDMS (3) and Au (6.9), respectively, d_{PDMS} and d_{Au} are the thickness of PDMS film (100 μm) and diameter of Au NP (15 nm), respectively. The σ'_{max} can be determined by the gap distance d_{gap} between top PDMS film and bottom electrode, because d_{PDMS}, d_{Au}, ε_{PDMS} and ε

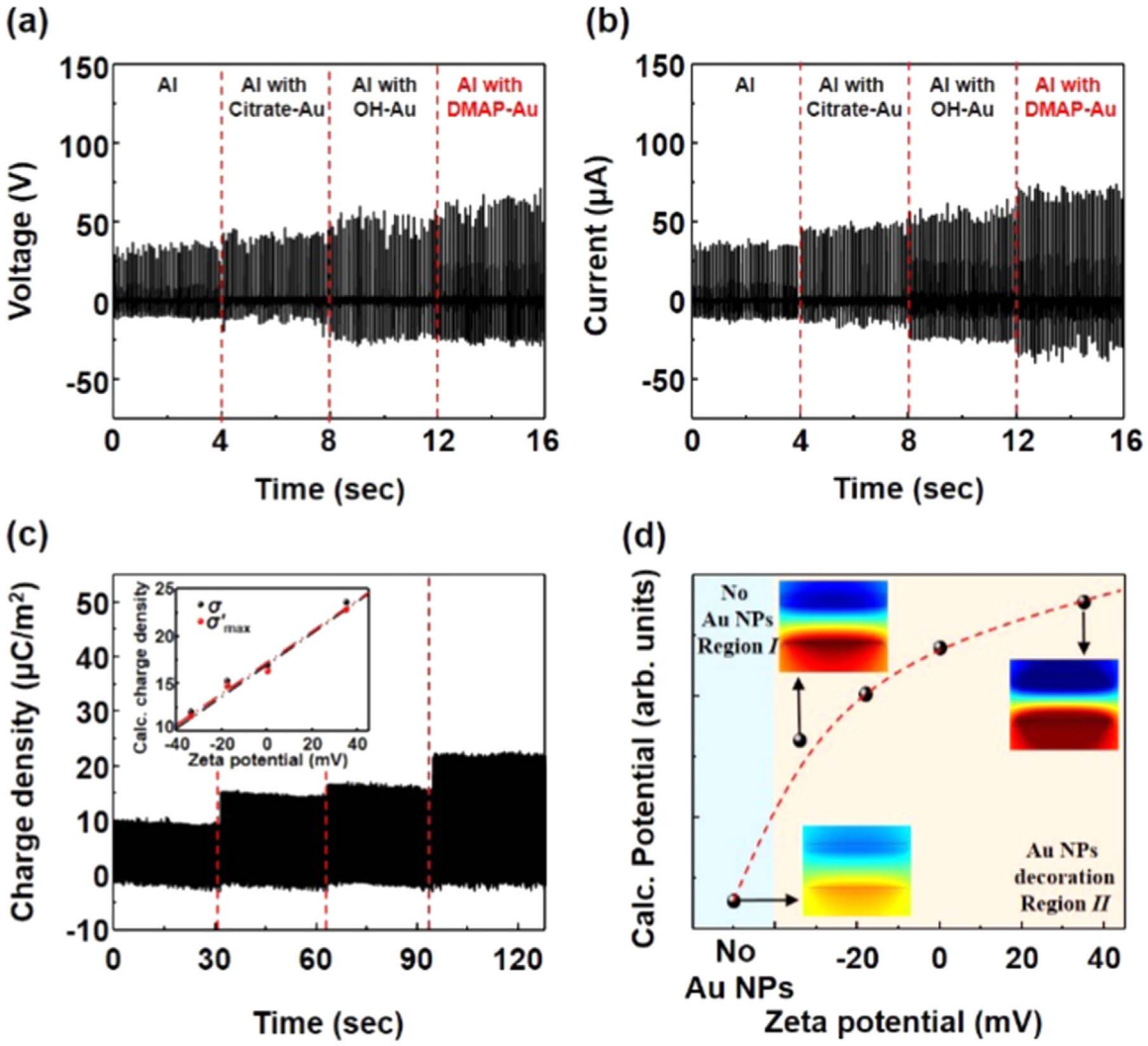

Fig. 7. (a) The output voltage and (b) current of the TENGs with pristine Al film and Al film decorated with Au NPs capped with Citrate, OH, and DMAP. (c) The measured transferred charge density. (d) The calculated electrostatic potentials of the TENGs with various capping agents, simulated by the COMSOL multi-physics software. The inset show potential distributions in the TENGs.

$_{Au}$ are constants. Therefore, the maximum surface charge densities on the top electrode of TENG with Au NPs capped with the DMAP, OH, and citrate can be obtained as σ'_{max} (DMAP)=21.86 μC/m^2, σ'_{max}(OH)=16.05 μC/m^2 and σ'_{max} (citrate)=14.60 μC/m^2 can be obtained, respectively. By using the COMSOL multi-physics software, we calculated electrostatic potentials of the Au NPs-decorated TENGs with the above results, as shown in Fig. 7d. It is clearly seen that TENG with Au NPs capped with the DMAP shows a large difference in electrostatic potentials, compared to those of TENGs with other capping agents. The enhancement was also observed when polyimide film, as a negative triboelectric material, was used, as plotted in Fig. S5.

In order to verify the increase of the transferred charge density, we measured the surface potential of polyimide films before and after friction with the OH- and DMAP-Au NPs, compared with the Al film. Fig. 8a shows the schematic illustration of KPFM system that measures the surface potential difference of the polyimide films compared to the tip before and after friction. Before the friction, the surface potential was measured to be approximately −134 mV, as shown in Fig. 8b. It was changed to −41 mV after the friction with the Al film (Fig. 8c), indicating that the electrons are transferred to the polyimide film. By DMAP-Au NPs, it was measured that the polyimide film had the surface potential of approximately 111 mV, larger 30 mV than that by OH-Au NPs (Fig. 8d and e). This clearly shows that more electrons are transferred to the polyimide film by the friction with DMAP-Au NPs.

4. Conclusions

In summary, we demonstrate a new way to enhance the charge transfer in a TENG based on contact-separation mode, by designing the positive triboelectric material which donate effectively electrons to the negative triboelectric materials, such as PDMS and polyimide. The keynote was to increase the stretchability for the uniform contact and to introduce a functional group for the surface potential control. Highly stretchable and conductive materials, consisting of the Ag NWs and PDMS, were suggested to make the uniform contact and proved to be effective. Here, the accurate control of the portion of the Ag NWs exposed above embedding surface was critical for the mechanical stability and the enhanced output power. To collect a large work function difference, a functional group such as positively charged DMAP on the surface of Au NPs was prepared by phase transfer method. By UPS measurement, it was clearly

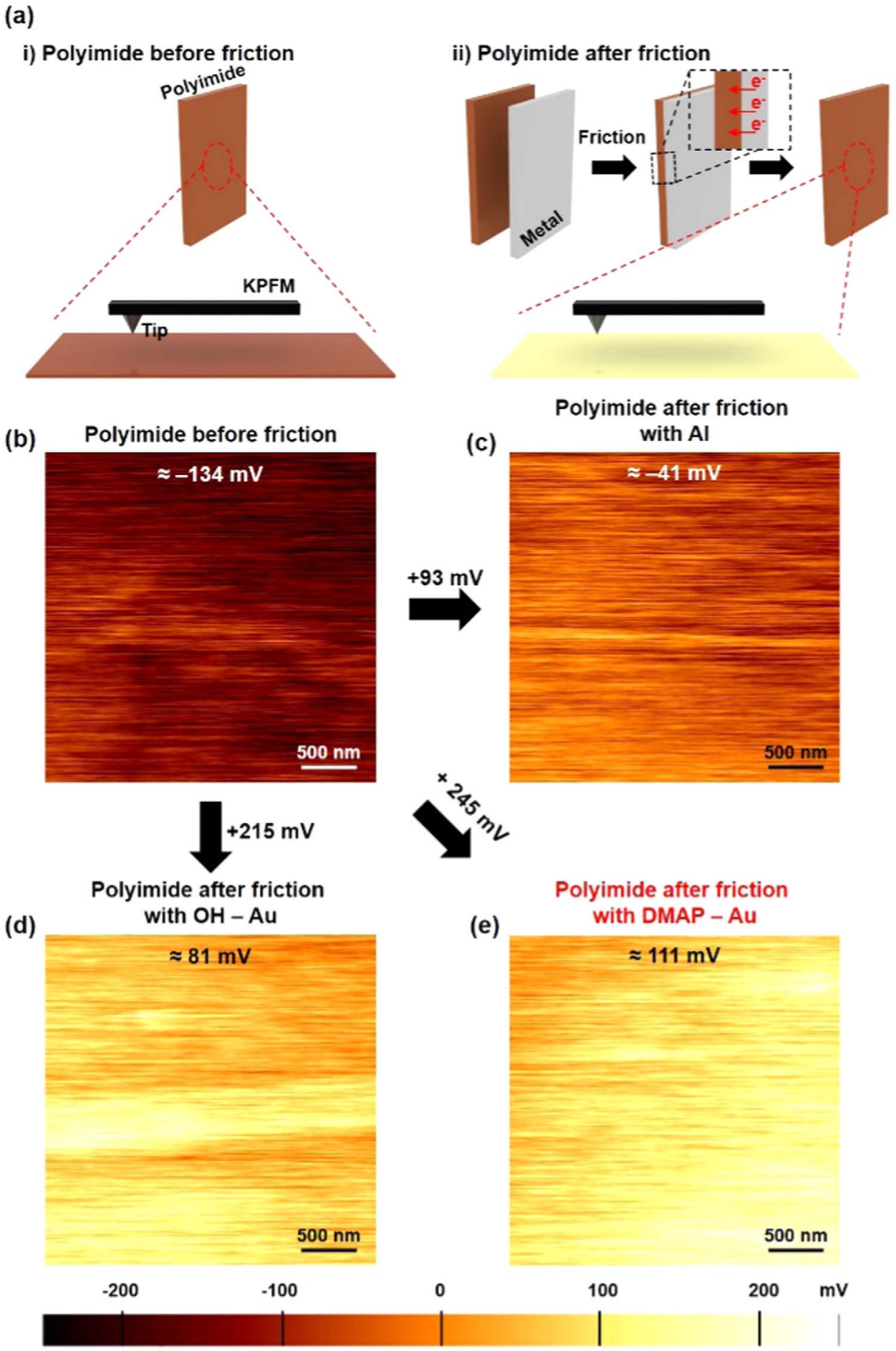

Fig. 8. (a) Schematic illustrations of KPFM experiments (b) The mean surface potential of polyimide film before friction. The surface potential of polyimide films after friction with (c) Al, (d) OH-Au, and (e) DMAP-Au.

observed that the DMAP lowered the effective work function of the Au NPs. This ascribes to the interfacial dipole within a few nanometers, induced from partial protonation of the exocyclic nitrogen atom that extends away from the surface of the Au NPs, thereby, increasing the potential difference with the negative triboelectric materials. This increased the transferred charge density on both surfaces, proved by KPFM measurement.

The designed TENG gives an output performance up to 80 V, 86 μA and 2.5 mW in output power, 2–2.5 times enhancement compared with the conventional TENGs. We also found a stable output performance from the TENG. With the integration with AC to DC converting circuit and buck-boost circuit, the TENG was demonstrated to produce a constant voltage of 2.6 V. The wireless sensing system was also demonstrated by the output voltage from the TENG, which operates the remote controller, resulted in turning on a siren of the system. It is believed that this work will serve as a stepping stone for high performance and stable TENG studies and will also inspire the big

development of the TENG towards self-powered electronics in the near future.

Acknowledgements

K. N. Kim and Dr. Y. K. Jung contributed equally to this work. This work was supported by Samsung Research Funding Center of Samsung Electronics under Project number SRFC-TA1403-06.

Appendix A. Supplementary material

Supplementary data associated with this article can be found in the online version at http://dx.doi.org/10.1016/j.nanoen.2016.05.048.

References

[1] L.B. Schein, Electrophotography and Development Physics, Laplacian, Morgan Hill, CA, 1996.
[2] D.M. Pai, B.E. Springett, Rev. Mod. Phys. 65 (1993) 163–211.
[3] B.A. Kwetkus, Part. Sci. Technol. 16 (1998) 55–68.
[4] F.-R. Fan, Z.-Q. Tian, Z.L. Wang, Nano Energy 1 (2012) 328–334.
[5] S. Wang, L. Lin, Z.L. Wang, Nano Lett. 12 (2012) 6339–6346.
[6] S. Wang, L. Lin, Y. Xie, Q. Jing, S. Niu, Z.L. Wang, Nano Lett. 13 (2013) 2226–2233.
[7] L. Lin, S. Wang, Y. Xie, Q. Jing, S. Niu, Y. Hu, Z.L. Wang, Nano Lett. 13 (2013) 2916–2923.
[8] C.K. Jeong, K.M. Baek, S. Niu, T.W. Nam, Y.H. Hur, D.Y. Park, G.-T. Hwang, M. Byun, Z.L. Wang, Y.S. Jung, K.J. Lee, Nano Lett. 14 (2014) 7031–7038.
[9] G. Cheng, Z.-H. Lin, L. Lin, Z.-l. Du, Z.L. Wang, ACS Nano 7 (2013) 7383–7391.
[10] G. Zhu, Z.-H. Lin, Q. Jing, P. Bai, C. Pan, Y. Yang, Y. Zhou, Z.L. Wang, Nano Lett. 13 (2013) 847–853.
[11] F.-R. Fan, L. Lin, G. Zhu, W. Wu, R. Zhang, Z.L. Wang, Nano Lett. 12 (2012) 3109–3114.
[12] K.Y. Lee, J. Chun, J.-H. Lee, K.N. Kim, N.-R. Kang, J.-Y. Kim, M.H. Kim, K.-S. Shin, M.K. Gupta, J.M. Baik, S.-W. Kim, Adv. Mater. 26 (2014) 5037–5042.
[13] S. Wang, Y. Xie, S. Niu, L. Lin, C. Liu, Y.S. Zhou, Z.L. Wang, Adv. Mater. 26 (2014) 6720–6728.
[14] X. Xue, Y. Fu, Q. Wang, L. Xing, Y. Zhang, Adv. Funct. Mater. 26 (2016) 3128–3138.
[15] S. Wang, Y. Zi, Y.S. Zhou, S. Li, F. Fan, L. Lina, Z.L. Wang, J. Mater. Chem. A 4 (2016) 3728–3734.
[16] S.-J. Park, M.-L. Seol, S.-B. Jeon, D. Kim, D. Lee, Y.-K. Choi, Sci. Rep. 5 (2015) 13866.
[17] M.-H. Yeh, H. Guo, L. Lin, Z. Wen, Z. Li, C. Hu, Z.L. Wang, Adv. Funct. Mater. 26 (2015) 1054–1058.
[18] Y. Jie, N. Wang, X. Cao, Y. Xu, T. Li, X. Zhang, Z.L. Wang, ACS Nano 9 (2015) 8376–8383.
[19] Q. Jing, G. Zhu, P. Bai, Y. Xie, J. Chen, R.P.S. Han, Z.L. Wang, ACS Nano 8 (2014) 3836–3842.
[20] Y. Xie, S. Wang, S. Niu, L. Lin, Q. Jing, J. Yang, Z. Wu, Z.L. Wang, Adv. Mater. 26 (2014) 6599–6607.
[21] B.-U. Hwang, J.-H. Lee, T.Q. Trung, E. Roh, D.-I. Kim, S.-W. Kim, N.-E. Lee, ACS Nano 9 (2015) 8801–8810.
[22] P.-K. Yang, L. Lin, F. Yi, X. Li, K.C. Pradel, Y. Zi, C.-I. Wu, J.-H. He, Y. Zhang, Z. L. Wang, Adv. Mater. 27 (2015) 3817–3824.
[23] D. Kim, S. Jeong, H. Shin, Y. Xia, J. Moon, Adv. Mater. 20 (2008) 3084–3089.
[24] M.D. Scanlon, P. Peljo, M.A. Mendez, E. Smirnov, H.H. Girault, Chem. Sci. 6 (2015) 2705–2720.
[25] S.-H. Oh, S.-I. Na, J. Jo, B. Lim, D. Vak, D.-Y. Kim, Adv. Funct. Mater. 20 (2010) 1977–1983.
[26] Y. Choi, M. Gu, J. Park, H.-K. Song, B.-S. Kim, Adv. Energy Mater. 2 (2012) 1510–1518.
[27] M. Brust, M. Walker, D. Bethell, D.J. Schiffrin, R. Whyman, J. Chem. Soc. Chem. Commun. (1994) 801–802.
[28] A.C. Templeton, W.P. Wuelfing, R.W. Murray, Acc. Chem. Res. 33 (2000) 27–36.
[29] A. Wijaya, K. Hamad-Schifferli, Langmuir 24 (2008) 9966–9969.
[30] N.R. Jana, L. Gearheart, C.J. Murphy, Langmuir 17 (2001) 6782–6786.
[31] P. Lee, J. Lee, H. Lee, J. Yeo, S. Hong, K.H. Nam, D. Lee, S.S. Lee, S.H. Ko, Adv. Mater. 24 (2012) 3326–3332.
[32] F. Xu, Y. Zhu, Adv. Mater. 24 (2012) 5117–5122.
[33] T. Cheng, Y.-Z. Zhang, W.-Y. Lai, Y. Chen, W.-J. Zeng, W. Huang, J. Mater. Chem. C 2 (2014) 10369–10376.
[34] A. Natan, Y. Zidon, Y. Shapira, L. Kronik, Phys. Rev. B. 73 (2006) 193310–193314.
[35] G. Zhu, C. Pan, W. Guo, C.-Y. Chen, Y. Zhou, R. Yu, Z.L. Wang, Nano Lett. 12 (2012) 4960–4965.

Kyeong Nam Kim is a Ph.D. candidate under the supervision of Prof. Jeong Min Baik at School of Materials Science and Engineering, Ulsan National Institute of Science and Technology (UNIST). His master's research focuses on development of composite and textile structure based piezoelectric generators/triboelectric generators for sustainable energy conversions, biocompatible device, and fundamental study.

Dr. Yun Kyung Jung is a research professor in School of Energy and Chemical Engineering, Ulsan National Institute of Science and Technology (UNIST). She received her Ph.D. from Department of Chemical and Biomolecular Engineering, Korea Advanced Institute of Science and Technology (KAIST). Her recent research interest is focused on polydiacetylene-based biosensor, drug delivery using carbon nanodots, cell imaging probe and triboelectric biosensor for self-powered in-field analysis.

Jinsung Chun is a Ph.D. candidate under the supervision of Prof. Jeong Min Baik at School of Materials Science and Engineering, Ulsan National Institute of Science and Technology (UNIST). His doctoral research focuses on development of ordered porous structure based piezoelectric generators/triboelectric generators for sustainable energy conversions, self-powered sensor, and fundamental study.

Byeong Uk Ye is a Ph.D. candidate under the supervision of Prof. Jeong Min Baik at School of Materials Science and Engineering, Ulsan National Institute of Science and Technology (UNIST). His doctoral research focuses on charge-enhancing mechanism with light-matter interaction in nano-phototronic devices for energy applications.

Minsu Gu is a Ph.D. candidate under the supervision of Prof. Byeong-Su Kim in the Department of Energy Engineering, Ulsan National Institute of Science and Technology (UNIST). As a receipent of the Global Ph.D. Fellowship from National Research Foundation of Korea, his current research interest is in electrochemistry of multilayer thin film electrodes for energy conversion and storage.

Eunyong Seo is a Ph.D. candidate under the supervision of Prof. Byeong-Su Kim in Department of Energy Engineering at Ulsan National Institute of Science and Technology (UNIST). He received his B.S. degree in Department of Polymer Engineering from Kyunghee University. He focused on the double hydrophilic block copolymer-templated nanomaterial synthesis and energy application. He is currently investigating the effect of polymer on the nanostructure synthesis through controlled block copolymer synthesis.

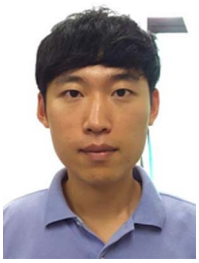

Seongsu Kim is a Ph.D. candidate under the supervision of Prof. Sang-Woo Kim at School of Advanced Materials Science & Engineering, Sungkyunkwan University (SKKU). His research interest includes the characterization study of 2D dimensional materials for the energy harvesting application.

Dr. Sang-Woo Kim is an Associate Professor in School of Advanced Materials Science and Engineering at Sungkyunkwan University (SKKU). He received his Ph. D. from Kyoto University in Department of Electronic Science and Engineering in 2004. After working as a postdoctoral researcher at Kyoto University and University of Cambridge, he spent 4 years as an assistant professor at Kumoh National Institute of Technology. He joined the School of Advanced Materials Science and Engineering, SKKU Advanced Institute of Nanotechnology (SAINT) at SKKU in 2009. His recent research interest is focused on piezoelectric/triboelectric nanogenerators, photovoltaics, and two-dimensional nanomaterials including graphene and hexagonal boron nitride nanosheets. Now he is an Associate Editor of Nano Energy and an Executive Board Member of Advanced Electronic Materials.

Dr. Byeong-Su Kim is an Associate Professor of Department of Chemistry at the Ulsan National Institute of Science and Technology (UNIST), Korea. He received his degrees in Chemistry from Seoul National University (BS 1999, MS 2001). In 2007, he received his Ph.D. in Polymer and Material chemistry at the University of Minnesota – Twin Cities. After a postdoctoral research at the Department of Chemical Engineering at MIT, he started his independent career at UNIST since August 2009. His research and education program cover a broad span of macromolecular chemistry in the study of novel polymer and hybrid nanomaterials, including the molecular design and synthesis of self-assembled polymers, layer-by-layer assembly for functional thin films, and now expand to complex macromolecular systems such as carbon nanomaterials for energy and biomedical applications.

Dr. Jeong Min Baik is now Associate Professor in School of Materials Science and Engineering, Ulsan National Institute of Science and Technology (UNIST). He received his Ph.D. from Pohang University in Department of Materials Science and Engineering in 2006. His recent research interest is focused on the synthesis of nanomaterials and nanostructures such as nanoparticles, nanowires, nanolayers, and nanopores for the applications of Energy-Conversion Devices and Nanophotonic Devices. Particular interests are concerned with the development of Piezoelectric/Triboelectric Nanogenerators and Artificial Photosynthesis.